Heteroepitaxial Streptavidin Nanocrystals Reveal Critical Role of Proton "Fingers" and Subsurface Atoms in Determining Adsorbed Protein Orientation

Daniel M. Czajkowsky,[†,‡,#] Lin Li,[†,#] Jielin Sun,[‡] Jun Hu,[†] and Zhifeng Shao[‡,*]

[†]Laboratory of Physical Biology, Shanghai Institute of Applied Physics, Chinese Academy of Sciences, Shanghai, China and, [‡]Key Laboratory of Systems Biomedicine (Ministry of Education) & State Key Laboratory of Oncogenes & Related Genes, Shanghai Jiao Tong University, Shanghai, China. [#]These authors contributed equally to this work.

ABSTRACT Characterization of noncovalent interactions between nanometer-sized structures, such as proteins, and solid surfaces is a subject of intense interest of late owing to the rapid development of numerous solid materials for medical and technological applications. Yet the rational design of these surfaces to promote the adsorption of specific nanoscale complexes is hindered by a lack of an understanding of the noncovalent interactions between nanostructures and solid surfaces. Here we take advantage of the unexpected observation of two-dimensional nanocrystals of streptavidin on muscovite mica to provide details of the streptavidin—mica interface. Analysis of atomic force microscopic images together with structural modeling identifies six positively charged residues whose terminal amine locations match the positions of the single atom-sized anionic cavities in the basal mica surface to within 1 Å. Moreover, we find that the streptavidin crystallites are oriented only along a single direction on this surface and not in either of three different directions as they must be if the protein interacted solely with the 3-fold symmetric basal surface atoms. Hence, this broken symmetry indicates that the terminal amine protons must also interact directly with the subsurface hydroxide atoms that line the bottom of these anionic cavities and generate only a single axis of symmetry. Thus, in total, these results reveal that subsurface atoms can have a significant influence on protein adsorption and orientation and identify the insertion of proton "fingers" as a means by which proteins may generally interact with solid surfaces.

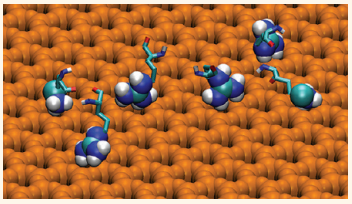

KEYWORDS: atomic force microscopy · protein adsorption · nanostructures · self-assembled · two-dimensional crystals · epitaxial growth

The development of nanometer-sized structures for technological and medical applications has exposed a poor understanding of how structures of this size generally interact with solid surfaces.[1−3] While van der Waals interactions can dominate interactions with microscopic objects and covalent bonding is usually exploited when working with single- or few-atom molecular interactions, it is generally believed that a complex mixture of van der Waals, electrostatic, and hydrogen-bonding interactions, which is different for different structures, is responsible for the noncovalent association of nanometer-sized objects with solid surfaces.[4−10]

The noncovalent adsorption of biological molecules, in particular, onto solid surfaces is in fact a long-known phenomenon that critically impacts the effectiveness of a wide range of biomedical and biotechnological devices.[2,11−15] For devices that operate within cellular fluids, protein adsorption is typically the first event that is observed when the device is placed within the biological environs and the one that can ultimately dictate its biological response.[11,16−19] For other biotechnological applications, such as protein microarrays and lab-on-a-chip devices, long-lived noncovalent protein adsorption remains an attractive possibility for specific immobilization of functional proteins.[20] In these cases, what is important is not just which proteins adsorb to the surfaces but also the orientation of the adsorbed species on the surface, as this determines the nature of the moieties that are exposed to the solvent and thus to the other biomolecules as well. One of the ultimate goals in the design of these devices is the rational preparation of surfaces that promote interactions with specific proteins in a specific orientation; yet this remains a significant challenge, as there is presently very little experimental information about the nature of the contacts between any protein with any solid surface.

* Address correspondence to zs9q@virginia.edu.

Received for review August 31, 2011 and accepted December 13, 2011.

Published online December 13, 2011
10.1021/nn203356p

Muscovite mica is an excellent model solid material to investigate details of protein adsorption, since it is atomically flat over distances of micrometers, has well-known surface properties, and has been empirically found to be a suitable substrate for many proteins in structural studies using atomic force microscopy (AFM).[21−47] This ability of many unrelated proteins to noncovalently associate with this surface suggests that there is a property of mica that may be mimicked in the design of surfaces for specific association with nanoscale structures. Moreover, in these AFM studies, a uniquely oriented species, with respect to the mica normal, is often observed.[21−27] Since this is found even for proteins that are, overall, neutral or negatively charged, such a uniquely oriented species underscores the selective and specific nature of association that must underlie interactions with the anionic mica substrate. The structures obtained in these AFM studies are often in excellent agreement with atomic models obtained from X-ray crystallography. Hence, AFM studies such as these could be used to reveal the identity of the protein regions that face the mica surface. If the specific protein structures could then be aligned with the underlying substrate structure, and the nature of physicochemical interactions identified, such an analysis would allow a dissection of the details of the protein−substrate interface.

We show here that the common biotin-binding protein streptavidin unexpectedly self-assembles into two-dimensional nanocrystals on the surface of muscovite mica. The adsorption characteristics of streptavidin to solid phase materials and biotinylated lipid monolayers/bilayers have previously been well studied for their tremendous biotechnological interest[48−51] and as model systems to better understand two-dimensional crystallization.[52,53] Yet, to our knowledge, heteroepitaxial crystallization of this protein has never been observed. Detailed analysis of the surface topography of these streptavidin crystals on mica together with structural modeling results in the identification of the mica-binding surface of the streptavidin molecule. Further, alignment with the underlying mica lattice establishes the registration of specific streptavidin residues with the mica surface. However it is a remarkable feature of the crystals—they are all oriented along a single direction on the mica surface—that enables a more detailed understanding of the protein−surface interactions associated with this specific streptavidin surface orientation.

RESULTS AND DISCUSSION

Streptavidin Spontaneously Forms 2D Crystallites on Mica. Direct application of streptavidin to mica results in its spontaneous adsorption to the substrate (Figure 1). Two different types of adsorbed species on this surface are clearly visible: proteins within islands of two-dimensional crystallites and a more loosely bound species that is readily moved aside by the scanning AFM tip. The latter property precludes a structural understanding of this species, but the crystals were sufficiently well adsorbed to withstand imaging forces even at smaller scan sizes, enabling a more detailed analysis of this crystal (Figure 1b). Each molecule within the crystal exhibits an essentially featureless, rounded surface topography (Figure 1b). The crystal dimensions are $a = 5.7 \pm 0.1$ nm, $b = 4.7 \pm 0.1$ nm, $\beta = 103 \pm 1°$, and the height from the mica lattice is 6.0 ± 0.1 nm (Figure 1c). It should also be noted that these crystal patches are markedly anisotropic, with the crystal along the *a*-axis on average 2.9 times ($n = 52$) longer than along the *b*-axis. This anisotropy endows the crystals with an easily identified directionality on the mica surface even at larger scan sizes (Figure 1a).

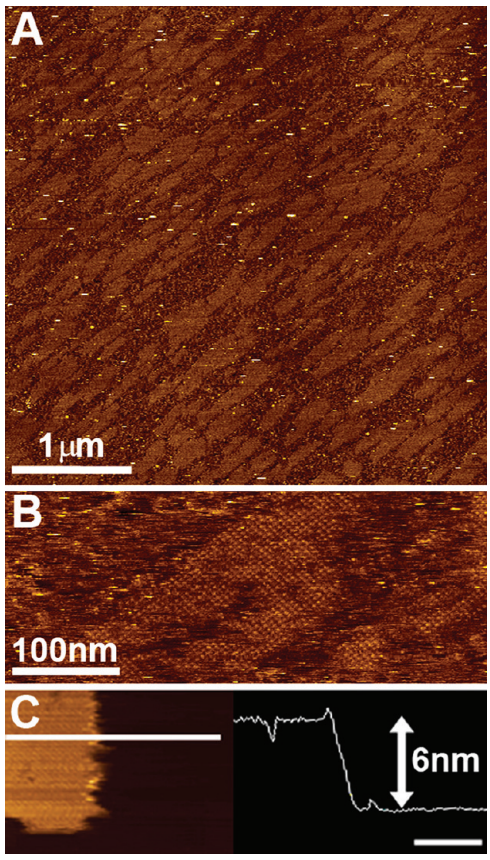

Figure 1. Streptavidin forms 2D crystals on mica. (A) Large scan size image showing many flat crystal islands, interspersed with more loosely bound protein. The crystals are limited in size and markedly anisotropic, with one crystal dimension significantly longer than the other. Each individual crystal patch is oriented on mica in the same direction. (B) Smaller scan size image showing individual streptavidin molecules within the crystal. The surface topography of the protein is simply that of a featureless protrusion. The unit cell dimensions are $a = 5.7 \pm 0.1$ nm, $b = 4.7 \pm 0.1$ nm, $\beta = 103 \pm 1°$. (C) At slightly greater imaging forces, the more loosely bound molecules can be moved away, enabling a measurement of the height of the proteins from the mica surface. The right panel shows the topographic profile along the white line in the left panel.

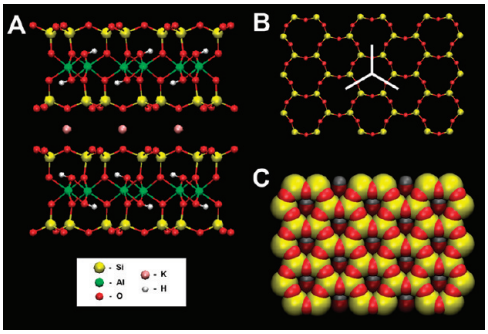

Figure 2. Crystal structure of muscovite mica. (A) Layered phylosilicate of 1 nm sheets with intercalated K atoms. (B) Cleaved [001] basal surface showing the 3-fold symmetry of the ditriagonal lattice of silicon and oxygen atoms. (C) VdW sphere representation of the [001] surface together with the sublayer of hydroxide atoms accessible through the atom-sized holes in the basal lattice. Not shown in this figure is the substitution of one Al^{3+} for every fourth Si^{4+} in the tetrahedral layer that endows this surface with an overall negative charge. There is no long-range order in this substitution.[54]

Streptavidin Crystals on Mica Are Oriented in a Singular Direction. The basal mica surface to which the proteins adsorb exhibits 3-fold symmetry owing to a slight distortion from a strictly hexagonal arrangement in the neighboring SiO_4 tetrahedra that delimit the atomic-sized, negatively charged cavities in this surface (Figure 2).[54,55] Hence, there are three equivalent directions in which the streptavidin crystals could form, assuming (as it is usually done) that the protein interacts exclusively with these surface atoms. However, all streptavidin crystal patches that we have observed are oriented in a single direction on the mica surface (Figure 1a, b). This was observed at both low and high crystal densities, between crystal patches that are up to 10 μm apart (the limit of the piezoscanner used), and with mica sheets from different sources (see Methods). It should also be noted that this singular orientation was not correlated with any specific direction of protein application and, thus, is not due to solution flow. In addition, the observed orientation of the crystal on mica was not dependent on the fast-scanning direction of the AFM tip (Figure S1). This singular direction of streptavidin crystal orientation indicates that the surface of mica with which the protein interacts does not, in fact, have the 3-fold symmetry of the basal surface atoms. To obtain a better understanding of this interaction, we sought to first identify the surface of streptavidin that faces mica and then the mica atoms to which this surface interacts.

Identification of the Orientation of Streptavidin on Mica. From the atomic model of streptavidin,[56] it is known that the tetramer has dihedral D_2 molecular symmetry, with molecular lengths of about 5.4, 5.9, and 4.8 nm along each diad axis, which we designate as *P*, *Q*, and *R*, respectively (Figure 3a).[57] Thus, from the crystal lattice constants and the measured height of the protein, the most likely orientation of streptavidin on the mica surface is with its *Q*-axis perpendicular to the mica surface and with the *R*-axis directly along the crystal *b*-axis (Figure 3a, left panel). This orientation is consistent with the observed surface topography (Figure 1b) and with an analysis of the electrostatic potential about the streptavidin protein, which shows that the side of the protein that faces the negatively charged mica is the most positively charged in the molecule (see below).

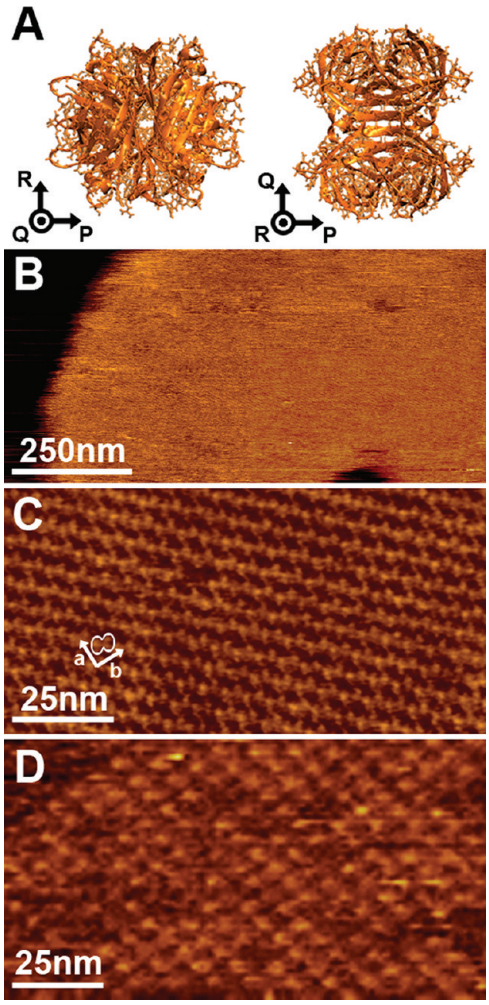

Figure 3. Identification of the orientation of streptavidin on mica. (A) Two views of the atomic model of streptavidin: along the diad Q-axis (see text), facing one of the two symmetrically equivalent most positively charged sides (left), and along the diad *R*-axis, facing one of the two symmetrically equivalent biotin-binding sides (right). (B and C) Streptavidin in two-dimensional crystals on supported lipid bilayers containing biotinylated lipids. (B) At large scan sizes, large crystal patches are readily observed on the supported bilayer. (C) At higher resolution, the surface topography of the protein resembles an hourglass, also consistent with the expected view of the molecule as depicted in the right image of A. The lattice constants of this crystal are $a = b = 7.9 \pm 0.1$ nm, $\beta = 92° \pm 3°$ ($n = 6$), consistent with previous studies.[58,59] (D) Higher resolution image of streptavidin on mica. Clearly the surface topography is different from that observed of the protein on the supported bilayer. Instead it is consistent with the expected view of the molecule depicted in the left image in A.

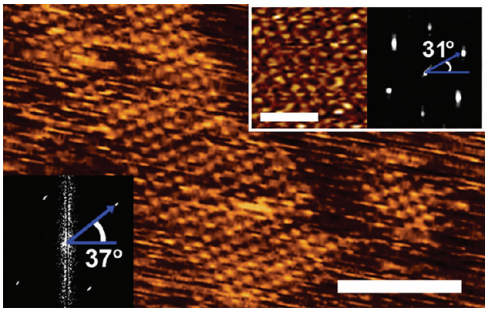

Figure 4. Identification of the relative orientation between the streptavidin and mica crystals. After obtaining a larger scan sized image of the streptavidin crystal (main panel), the immediately adjacent bare mica surface was imaged at a smaller scan size (upper right panel). As shown in the insets to both panels, the Fourier transforms of both crystals show that the streptavidin *b*-axis is 6° from lying exactly along one of the mica axes. Scale bars: main panel, 50 nm; upper panel, 2 nm.

The topographic profile and lattice dimensions of the streptavidin crystals on mica are also completely different from those of the streptavidin crystals on biotinylated lipid bilayers (Figure 3c, d), which exhibit the expected hourglass shape of individual molecules oriented with their biotin-binding side facing the bilayer.[58,59] Since the biotin-binding side is normal to the *R*-axis, these differences with the protein bound to biotinylated bilayers are thus also consistent with the proposed mica orientation.

Determination of the Streptavidin-Binding Sites on Mica. With the protein thus oriented within the crystallite and with respect to the mica plane, we sought to determine the orientation of the protein within the mica plane, that is, relative to the underlying mica lattice. To this end, we first obtained an image of the streptavidin crystal and then immediately imaged an adjacent region of bare mica at smaller scan sizes (Figure 4). In this way, we found that one of the mica axes is rotated slightly ($5 \pm 2°$, $n = 12$) away from the *b*-axis of the streptavidin crystal (inset, Figure 4) and thus also from the *R*-axis of the protein.

Together, the results described so far indicate that streptavidin is orientated with its *Q*-axis perpendicular to the mica surface and its *R*-axis rotated by about 5° from one of the mica axes. Inspection of this mica-binding side in the atomic model of streptavidin[56] reveals six positively charged residues that can directly interact with mica (Figure 5a). These are Arg53, Arg 59, and Lys80 in both subunits on this side. These residues are not only sufficiently surface exposed to simultaneously contact mica but also positioned so that their terminal amines could simultaneously interact with the anionic cavities in the mica lattice (Figure 5b). There is, in fact, one terminal proton of each of these residues that is within 1 Å of a cavity in the mica lattice in this depiction, which is a remarkable overlap between the mica lattice and the 3D-crystallographically determined structure of the protein.

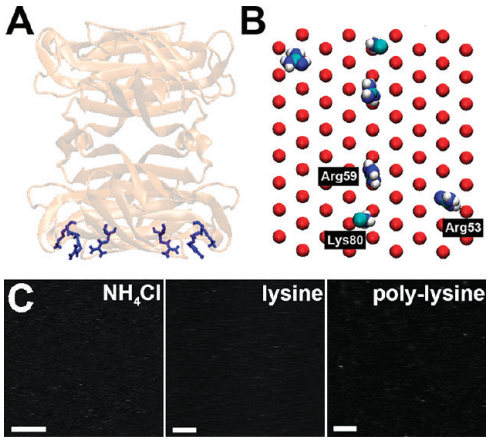

Figure 5. Positively charged residues in streptavidin that match the lattice of holes in the basal mica surface. (A) Six basic residues on one of the symmetrically equivalent protein surfaces that are suggested to directly face mica are shown in stick representation. (B) These residues are found to be well positioned to simultaneously interact with the mica lattice holes. The terminal moieties of each residue are shown as vdW spheres (cyan, carbon; blue, nitrogen; white, hydrogen), as are the sublayer hydroxide oxygen atoms of the mica lattice. (C) Solutions containing 1 mM of each of ammonium chloride, lysine, and polylysine are found to inhibit binding of streptavidin to mica. Scale bar, 200 nm.

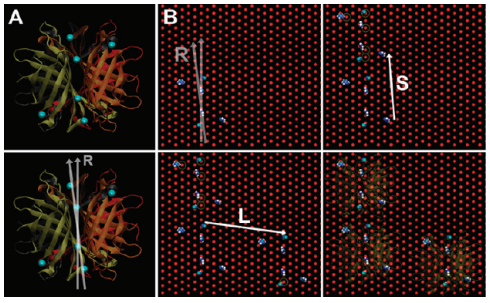

Figure 6. Source of mismatch producing streptavidin crystals of unequal dimensions. (A) On the mica-binding face of streptavidin, one set of four charged residues forms an "axis" of basic charge. This axis is slightly displaced from the diad *R*-axis. (B) Protein−protein contacts in the crystal along the shorter direction (S) occur along this *R*-axis, but contact with mica occurs such that the axis of basic charge is precisely along one mica lattice direction. Simple displacement along the mica lattice would satisfy the interactions with mica, but not the protein−protein interactions. Translation along the molecular *R*-axis thus displaces the axis of basic charge from the mica lattice. The yellow rings show the atoms with which the protein would have interacted with a simple translation. Some of the residues may still interact within the mica holes, but not as well as in first protein. Translating the protein in the long crystal dimension (L) gives a much lower degree of mismatch, as shown in the lower right panel.

Further, four of these charged residues effectively form an axis of positive charge on this surface that is ~7° away from the molecular *R*-axis (Figure 6a), similar to the amount by which the molecular *R*-axis is observed to be rotated from the mica axis. This means that it is possible for growth to occur along the *b*-axis direction in such a way that this axis of positive charge

in each additional molecule is similarly aligned with the mica axis (Figure 6b). However, translation along the molecular *R*-axis by the measured lattice distance would be expected to cause a somewhat significant displacement of these residues from the mica positions with which they would otherwise have been associated with a simple translation directly along the mica axis (Figure 6b). There is also a mismatch upon translating in the longer (10) crystal direction by the observed amount (Figure 6b), but this is not as significant as in the (01) direction. This greater mismatch along the *a*-axis than along the *b*-axis is likely responsible for the observed crystal shape anisotropy (Figure 1b).

The favorable electrostatic energy of the six positively charged protons within six negatively charged holes in the basal surface is substantial (~24 kT; see Methods). Further, free energy calculations reveal that the protein surfaces involved in intermolecular contacts within the crystal do not exhibit more than ~3 kT favorable energy, indicating that these interactions, alone, do not play a dominant role in their interaction on the mica surface (see Methods). Hence, these six charged residues are thus likely to account for a significant portion of the favorable energy determining streptavidin adsorption and orientation to mica. To further verify this idea, we expected that a solution of similar amine moieties should compete with streptavidin for binding to mica, as these both would bind to precisely the same region of mica. We thus incubated 1 mM solutions each of NH_4Cl, lysine, or polylysine, prior to the addition of streptavidin, and as Figure 5c shows, each of these molecules clearly inhibited the binding of streptavidin to mica. The crystal density on mica was also pH dependent, decreasing above pH 7 to zero at pH 11 (Figure S2), also consistent with an important role of these positively charged residues (particularly lysine with pK_a 9−10) in the interaction with mica.

Streptavidin Inserts within the Basal Layer Holes in Mica. These results are thus consistent with the streptavidin molecule interacting with the mica surface such that a single proton from each of these six positively charged residues directly interacts with the cavities within the mica lattice. Yet, this interaction with the cavities of the mica lattice also provides a means to explain how the entire crystal can be singularly oriented on the mica surface. The bottom of these cavities consists of a hydroxide molecule that is inclined by 20° in a single direction (toward the "empty cell" in the octahedral layer[60]) (Figure 2 and Figure 7). Moreover, the oxygen atom of the hydroxide is also not located exactly in the center but is slightly off to one side (Figure 7a). As a result, the basal mica surface atoms, together with these hydroxide atoms, exhibit only a singular axis of symmetry (along the projection of the hydroxide vector in the basal plane) (Figure 7b, c). Therefore, interaction of the protons on the terminal amines with

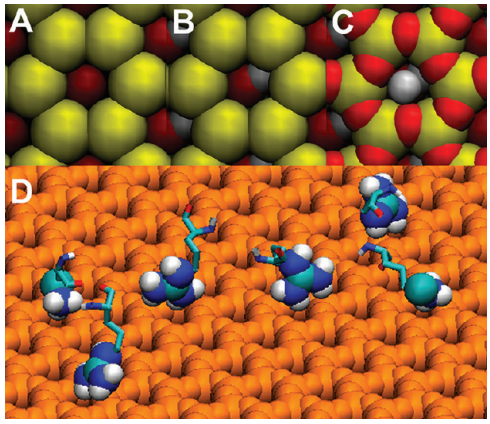

Figure 7. Source of anisotropy in crystal orientation on the mica lattice. (A) The hydroxide oxygen atom in the sublayer is not precisely in the middle of the hole, but is slightly off-center. Only the silicon atoms in the basal surface are shown for clarity. (B) The hydroxide hydrogen is oriented in a specific direction (toward the vacancy in the underlying octahedral layer), slightly inclined to the hole. (C) Both of these effects force the protein proton to bind off-center within the hole, in a direction directly opposite the hydroxide vector. The atoms are colored as in Figure 2. (D) The possible ways by which the terminal amine protons can insert into the mica cavities are limited geometrically by the other residue atoms as well as by the allowable torsions of the residues. The terminal amines are shown in vdW spheres, with the other residue atoms as stick representations. In this figure, protons are white, nitrogen is blue, carbon is cyan, oxygen is red, and all of the mica atoms are orange.

these singularly directed hydroxide molecules breaks the 3-fold symmetry of an exclusive interaction with basal surface atoms. It should be noted that the possible ways by which these terminal amine protons can insert within these cavities is limited geometrically by the other residue atoms as well as by the allowable torsions of the residues (Figure 7d). These residues are also located within beta strand secondary structures, and not loops, which also limits their flexibility. An estimation of the energy differences associated with this limited flexibility (see Methods) indeed reveals significant energetic differences (of tens of kcal/mol) that would be associated with the different directions. Hence, the observed singularly directed crystal growth is a consequence of both the direct interaction with the subsurface hydroxides and the limited number of possible ways by which the terminal protons from these six residues can be simultaneously inserted within the cavities.

Similar Charge Pattern in Other Mica-Binding Proteins. As mentioned in the introduction, muscovite mica is a frequently used substrate for structural studies of proteins with AFM. In previous work, we demonstrated that the (unrelated) bacterial proteins cholera toxin B-pentamer (CTB) and pertussis toxin B-pentamer (PTB) bind tightly to mica in a unique orientation, namely, with their A-subunit-binding surfaces exposed to solution.[22,26,27,61] Thus, with their surface

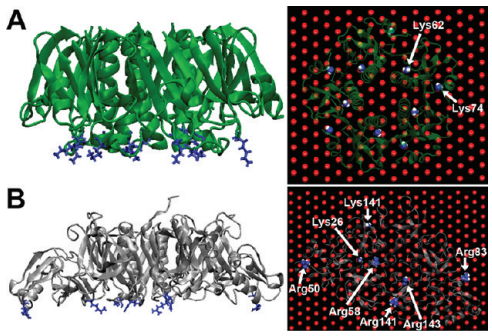

Figure 8. Positively charged residues on the mica-facing surfaces of other proteins also match the lattice of cavities in mica. (A) The cholera toxin B-oligomer binds to mica with its A-subunit binding surface exposed to solution.[22,26,27,61] Inspection of the crystal structure[62] of the mica-binding surface reveals two lysine residues per oligomer (right panel) that are well positioned to simultaneously contact mica cavities. (B) The pertussis toxin B-oligomer also binds to mica with its A-subunit binding surface exposed to solution. The mica-binding surface of the crystal structure[63] shows seven positively charged residues whose terminal amines are all within 1 Å of a mica cavity (right panel).

orientations established, we inspected the mica-binding surfaces of the atomic models of these proteins to determine whether the mechanism of interaction with mica observed with streptavidin might also play a role in adsorption with these proteins. As Figure 8 shows, the mica-binding surface of CTB[62] has 10 lysine residues, nine of which are within 1 Å of the mica cavities, while the mica-binding surface of PTB[63] has seven positively charged residues that are within 1 Å of the mica cavities. Thus, just as with streptavidin, adsorption of these proteins to mica also appears to be due to the spatial pattern of charged residues on one of its surfaces that matches the spatial arrangement of anionic mica cavities. However, it should also be noted that five of these nine CTB residues, and all of these PTB residues, are located in random loops, unlike the cationic residues in streptavidin located within the more ordered beta strands. This difference might contribute to the more random distribution, within the mica plane, of CTB and PTB compared with streptavidin.

CONCLUSION

We have provided structural information on the interface between a protein and a solid surface to a higher level of experimental detail than previously described. Streptavidin interacts not only with the topmost layer of atoms in this solid but also with the hydroxide atoms beneath this topmost layer, as it inserts proton "fingers" from cationic residues into the atomic-sized holes within the basal surface. This latter detail, revealing not just a lateral spatial charge matching but also a third-dimensional structural dependence (the insertion of the protein protons), illustrates a previously unnoticed contribution of shape complementarity between the protein and substrate surface in protein, and other nanometer-sized structures, adsorption. As surfaces like mica have been suggested to serve as templates to seed the growth of three-dimensional protein crystals,[64,65] it is important to take this unique interaction into account in the search for the optimal crystallization conditions. Similarly, this type of interaction might also provide a plausible explanation for the difficulties of using crystalline surfaces to promote the formation of well-ordered protein crystals, even when apparent lattices seem to fit. More generally, as atomic-sized defects are likely a common feature of many solid surfaces, this aspect of ultimate contact might likewise be a common means of protein attachment to many surfaces. Thus, it is necessary to understand the roughness of a particular solid surface, even down to the atomic level, in order to properly predict the adsorption of a specific protein. Along the same lines, if the structure of a given protein is known, it should be possible to construct specific surfaces that would match the unique charge and surface topography of this protein to promote its attachment, with the recent advances in synthetic self-assembled structures.[66,67] Of particular importance for this development would be those charged residues located within more structurally ordered secondary structure elements compared with random loops, as these might be a more specific characteristic of the particular protein. Finally, although this interaction was observed on a large surface, similar interactions are undoubtedly also important for the adsorption of proteins to nanoparticles, where it is well known that the tightly adsorbed protein is thought to be ultimately responsible for its biological effects.[3,8,18,19] The increased stress within the particles[68] as well as their small radius of curvature would both be expected to favor small defects on these surfaces as a mechanism to relieve stress. While it may be experimentally challenging in the near future to determine the precise means by which proteins contact nanoparticle surfaces, it should be possible to obtain some insight from theoretical calculations once these are improved to accurately account for the binding of proteins to larger surfaces. For the latter, the observations described in the present report would serve as a useful benchmark.

MATERIALS AND METHODS

Preparation and AFM Imaging of Samples on Mica. Most of the samples of streptavidin (Sigma, Shanghai, China) on mica were prepared by cleaving muscovite mica with tape and then applying the streptavidin solution (1.7 μM, final concentration, in deionized water) to the new surface. After incubating for 30 min, the sample was placed within the AFM (Nano III, Veeco)

and imaged in the contact mode using oxide-sharpened "twin-tip" Si_3N_4 cantilevers, with a spring constant of 0.06 N/m. The scan rate was 8 Hz and the applied force was minimized to 0.1 nN. The piezoscanner was calibrated by imaging the mica surface and a calibration grid (Veeco). Identical results were observed with mica obtained from Ted Pella, Inc. or from Mei Feng Industry, LLC, China. The samples with ammonium chloride (Sinopharm Chemical Reagent Co., Ltd., Shanghai, China), lysine (Bio Basic Inc., Canada), and polylysine (Sigma, Shanghai, China) were prepared by first incubating the freshly cleaved mica surface with 1 mM solutions of either of these chemicals for 30 min, followed by a brief rinsing of the surface and the removal of nearly all of this solution (leaving a very thin film on the surface), then addition of streptavidin (1.7 μM) in 1 mM solutions of the chemicals and incubation for 30 min. Following this procedure with only water (that is, without the amine chemicals) yielded results identical to those obtained following the aforementioned more commonly followed procedure. This preincubation with the amine chemical solutions was followed to ensure sufficient binding, if any, to avoid any possible complications of differences in kinetics on the results.[28]

Preparation of Streptavidin Crystals on Supported Lipid Bilayers. To prepare the samples of streptavidin on supported biotinylated lipid bilayers, the supported lipid bilayer was first prepared using the standard vesicle fusion procedure.[37,58,69] Briefly, 1,2-dioleoyl-*sn*-glycero-3-phosphocholine, 1-palmitoyl-2-linoleoyl-*sn*-glycero-3-phospho-L-serine, and 1,2-dipalmitoyl-*sn*-glycero-3-phosphoethanolamine-*N*-(cap biotinyl) (9.4:2.7:1 mol, 0.1 mg/mL in 2 mM $CaCl_2$, 150 mM NaCl, 10 mM HEPES, pH 7.4, Avanti Polar Lipids) were first dissolved in water and sonicated in a bath sonicator until the solution became clear (usually 4 h). This solution was then deposited on the freshly cleaved mica surface and incubated for 1 h. The sample was then rinsed with the same buffer, and then streptavidin was added to a final concentration of 1.7 μM. After an incubation period of 1 h, the sample was imaged. For some of the samples, the buffer was changed to 80 mM KCl, 10 mM Tris-HCl, pH 8.0, which seemed to enable more stable imaging, but which otherwise produced similar results to those with the first solution.

Estimation of the Protein–Mica Energy, the Interaction Free Energy between Two Proteins, and the Energy Differences of Differently Oriented Proteins. An approximate measure of the energy between the six charged residues per streptavidin and the mica substrate was determined by calculating the electrostatic energy between two point charges (a protein proton and the mica anionic charge) and then multiplying by six. The charge within the basal mica surface arises from the substitution of one Al^{3+} for every fourth Si^{4+} in the tetrahedral layer. The excess negative charge is thus likely distributed equally among the associated tetrahedral oxygen atoms, but for our approximate calculation, we assumed the charge was equally distributed within the three nearest oxygen atoms to the center of each cavity, the assumed position of the protein proton.

The free energy between proteins was calculated using the adaptive biasing force method[70] in NAMD[71,72] using the CHARMM27 force field.[73] The crystal structure of streptavidin[56] was first solvated in TIP3 water,[74] minimized, and then equilibrated. Two calculations were performed: one that determined the free energy profile between two equilibrated streptavidin molecules along the *a*-axis and one for a pair of molecules along the *b*-axis. In both calculations, one molecule was held fixed (by fixing the locations of four residues on the side opposite that which interacts with the other molecule) while the other molecule was constrained to move only along a single direction that corresponds to either the *a*- or *b*-axis (by constraining the four carbon backbone atoms of Trp108 in the tetramer to motions only along this direction). The molecules were otherwise free to move. For the calculations along the *a*-axis, the fixed residues were Ala50 on two monomers (of the tetramer) and Thr66 on the other two monomers. For the calculations along the *b*-axis, Glu44 and Gly68 were each held fixed on two monomers. Separate calculations were performed within distance ranges of 0.15 nm from 4.85 to 6.75 nm along the *a*-direction and from 4.45 to 5.65 nm along the *b*-direction. The results from each of these 0.15 nm sections were then combined to yield the profile along the full range. The free energy associated with crystal contacts was determined by calculating the difference between the energies at the crystal dimensions (a = 5.7 nm and b = 4.7 nm) and at the furthest distances between molecules. The figures with the atomic models were generated using VMD.[71]

The energy differences between proteins that interact with the mica surface in directions that differ by 120° within the mica plane were calculated as follows. As described in the text, there are geometrical limitations to the potential ways by which the amine protons can insert resulting from the other residue (and protein) atoms. An estimation of the differences in energy associated with these limitations was determined by assuming that, for each of the six residues, the orientation of the terminal amine nearest to the mica cavity (in the overlap with the mica lattice) was the proper orientation for the interaction with mica. A protein that differs by 120° on the mica surface from the original direction would then require each of the terminal amines to be rotated by 120° in the opposite direction to establish the identical contact with the mica cavity as in the original direction. Thus, to calculate the differences in energy, each of the six residues was individually rotated by 120° and centered at the inserting proton, and then the energies, minimized by conjugate gradients using NAMD, were computed. Each of the two possible 120° rotations was calculated, and the differences in minimized energy, from the original orientation, were 24 and 67 kcal/mol, respectively, for the two orientations.

Acknowledgment. This work was supported by NSFC (11074168, 91027020, and 60907044), MOST (2007CB936000, 2012CB932600), Shanghai Municipal Science and Technology Commission (1052 nm07700, 10PJ1405100), and the Chinese Academy of Sciences (No. KJCX2-EW-N03). D.M.C. was supported by the Chinese Academy of Sciences Fellowships for Young International Scientists (2009YA1-1). Z.S. acknowledges support from K.C. Wong Foundation (H.K.).

Supporting Information Available: Images obtained at different fast scan directions relative to the crystal orientation and results of the pH dependence of the crystal density. This material is available free of charge *via* the Internet at http://pubs.acs.org.

REFERENCES AND NOTES

1. Carrillo, J. M. Y.; Dobrynin, A. V. Layer-by-Layer Assembly of Charged Nanoparticles on Porous Substrates: Molecular Dynamics Simulations. *ACS Nano* **2011**, *5*, 3010–3019.
2. Gray, J. J. The Interaction of Proteins with Solid Surfaces. *Curr. Opin. Struct. Biol.* **2004**, *14*, 110–115.
3. Park, S.; Hamad-Schifferli, K. Nanoscale Interfaces to Biology. *Curr. Opin. Chem. Biol.* **2010**, *14*, 616–622.
4. Bachmann, M.; Goede, K.; Beck-Sickinger, A. G.; Grundmann, M.; Irback, A.; Janke, W. Microscopic Mechanism of Specific Peptide Adhesion to Semiconductor Substrates. *Angew. Chem., Int. Ed.* **2010**, *49*, 9530–9533.
5. Basalyga, D. M.; Latour, R. A. Theoretical Analysis of Adsorption Thermodynamics for Charged Peptide Residues on SAM Surfaces of Varying Functionality. *J. Biomed. Mater. Res., Part A* **2003**, *64A*, 120–130.
6. Kubiak-Ossowska, K.; Mulheran, P. A. Mechanism of Hen Egg White Lysozyme Adsorption on a Charged Solid Surface. *Langmuir* **2010**, *26*, 15954–15965.
7. Nel, A. E.; Madler, L.; Velegol, D.; Xia, T.; Hoek, E. M. V.; Somasundaran, P.; Klaessig, F.; Castranova, V.; Thompson, M. Understanding Biophysicochemical Interactions at the Nano-Bio Interface. *Nat. Mater.* **2009**, *8*, 543–557.
8. Rabe, M.; Verdes, D.; Seeger, S. Understanding Protein Adsorption Phenomena at Solid Surfaces. *Adv. Colloid Interface Sci.* **2011**, *162*, 87–106.
9. Arce, F. T.; Jang, H.; Ramachandran, S.; Landon, P. B.; Nussinov, R.; Lal, R. Polymorphism of Amyloid β Peptide in Different Environments: Implications for Membrane Insertion and Pore Formation. *Soft Matter* **2011**, *7*, 5267–5273.

10. Liu, F.; Arce, F. T.; Ramachandran, S.; Lal, R. Nanomechanics of Hemichannel Conformations. *J. Biol. Chem.* **2006**, *281*, 23207–23217.
11. Anderson, J. M.; Rodriguez, A.; Chang, D. T. Foreign Body Reaction to Biomaterials. *Semin. Immunol.* **2008**, *20*, 86–100.
12. Ratner, B. D.; Bryant, S. J. Biomaterials: Where We Have Been and Where We Are Going. *Annu. Rev. Biomed. Eng.* **2004**, *6*, 41–75.
13. Sanavio, B.; Scaini, D.; Grunwald, C.; Legname, G.; Scoles, G.; Casalis, L. Oriented Immobilization of Prion Protein Demonstrated via Precise Interfacial Nanostructure Measurements. *ACS Nano* **2010**, *4*, 6607–6616.
14. Sund, J.; Alenius, H.; Vippola, M.; Savolainen, K.; Puustinen, A. Proteomic Characterization of Engineered Nanomaterial-Protein Interactions in Relation to Surface Reactivity. *ACS Nano* **2011**, *5*, 4300–4309.
15. Lv, S.; Dudek, D. M.; Cao, Y.; Balamurali, M. M.; Gosline, J.; Li, H. B. Designed Biomaterials to Mimic the Mechanical Properties of Muscles. *Nature* **2010**, *465*, 69–73.
16. Cedervall, T.; Lynch, I.; Lindman, S.; Berggard, T.; Thulin, E.; Nilsson, H.; Dawson, K. A.; Linse, S. Understanding The Nanoparticle-Protein Corona Using Methods to Quantify Exchange Rates and Affinities of Proteins for Nanoparticles. *Proc. Natl. Acad. Sci. U. S. A.* **2007**, *104*, 2050–2055.
17. Linse, S.; Cabaleiro-Lago, C.; Xue, W. F.; Lynch, I.; Lindman, S.; Thulin, E.; Radford, S. E.; Dawson, K. A. Nucleation of Protein Fibrillation by Nanoparticles. *Proc. Natl. Acad. Sci. U. S. A.* **2007**, *104*, 8691–8696.
18. Lynch, I.; Cedervall, T.; Lundqvist, M.; Cabaleiro-Lago, C.; Linse, S.; Dawson, K. A. The Nanoparticle—Protein Complex as A Biological Entity; A Complex Fluids and Surface Science Challenge for The 21st Century. *Adv. Colloid Interface Sci.* **2007**, *134—35*, 167–174.
19. Lynch, I.; Salvati, A.; Dawson, K. A. Protein-Nanoparticle Interactions: What Does the Cell See?. *Nat. Nanotechnol.* **2009**, *4*, 546–547.
20. Zhu, H.; Snyder, M. Protein Chip Technology. *Curr. Opin. Chem. Biol.* **2003**, *7*, 55–63.
21. Czajkowsky, D. M.; Iwamoto, H.; Cover, T. L.; Shao, Z. F. The Vacuolating Toxin from Helicobacter pylori Forms Hexameric Pores in Lipid Bilayers at Low pH. *Proc. Natl. Acad. Sci. U. S. A.* **1999**, *96*, 2001–2006.
22. Czajkowsky, D. M.; Shao, Z. F. Submolecular Resolution of Single Macromolecules with Atomic Force Microscopy. *FEBS Lett.* **1998**, *430*, 51–54.
23. Han, W. H.; Mou, J. X.; Sheng, J.; Yang, J.; Shao, Z. F. Cryo Atomic Force Microscopy—A New Approach for Biological Imaging at High Resolution. *Biochemistry* **1995**, *34*, 8215–8220.
24. Mou, J. X.; Czajkowsky, D. M.; Sheng, S. J.; Ho, R. Y.; Shao, Z. F. High Resolution Surface Structure of E-Coli GroES Oligomer by Atomic Force Microscopy. *FEBS Lett.* **1996**, *381*, 161–164.
25. Mou, J. X.; Sheng, S. T.; Ho, R. Y.; Shao, Z. F. Chaperonins GroEL and GroES: Views from Atomic Force Microscopy. *Biophys. J.* **1996**, *71*, 2213–2221.
26. Yang, J.; Mou, J. X.; Shao, Z. F. Structure and Stability of Pertussis Toxin Studied by In-Situ Atomic Force Microscopy. *FEBS Lett.* **1994**, *338*, 89–92.
27. Yang, J.; Tamm, L. K.; Tillack, T. W.; Shao, Z. New Approach for Atomic Force Microscopy of Membrane Proteins—The Imaging of Cholera Toxin. *J. Mol. Biol.* **1993**, *229*, 286–290.
28. Czajkowsky, D. M.; Shao, Z. Inhibition of Protein Adsorption to Muscovite Mica by Monovalent Cations. *J. Microsc.* **2003**, *211*, 1–7.
29. Bippes, C. A.; Muller, D. J. High-Resolution Atomic Force Microscopy and Spectroscopy of Native Membrane Proteins. *Rep. Prog. Phys.* **2011**, *74*, 8.
30. Epand, R. M.; Maekawa, S.; Yip, C. M.; Epand, R. F. Protein-Induced Formation of Cholesterol-Rich Domains. *Biochemistry* **2001**, *40*, 10514–10521.
31. Hansma, H. G.; Laney, D. E. DNA Binding to Mica Correlates with Cationic Radius: Assay by Atomic Force Microscopy. *Biophys. J.* **1996**, *70*, 1933–1939.
32. Hoh, J. H.; Sosinsky, G. E.; Revel, J. P.; Hansma, P. K. Structure of the Extracellular Surface of the Gap Junction by Atomic Force Microscopy. *Biophys. J.* **1993**, *65*, 149–163.
33. Kasas, S.; Thomson, N. H.; Smith, B. L.; Hansma, H. G.; Zhu, X. S.; Guthold, M.; Bustamante, C.; Kool, E. T.; Kashlev, M.; Hansma, P. K. Escherichia coli RNA Polymerase Activity Observed Using Atomic Force Microscopy. *Biochemistry* **1997**, *36*, 461–468.
34. Muller, D. J.; Amrein, M.; Engel, A. Adsorption of Biological Molecules to a Solid Support for Scanning Probe Microscopy. *J. Struct. Biol.* **1997**, *119*, 172–188.
35. Rivetti, C.; Guthold, M.; Bustamante, C. Scanning Force Microscopy of DNA Deposited onto Mica: Equilibration Versus Kinetic Trapping Studied by Statistical Polymer Chain Analysis. *J. Mol. Biol.* **1996**, *264*, 919–932.
36. Scheuring, S.; Sturgis, J. N. Chromatic Adaptation of Photosynthetic Membranes. *Science* **2005**, *309*, 484–487.
37. Shao, Z. F.; Mou, J.; Czajkowsky, D. M.; Yang, J.; Yuan, J. Y. Biological Atomic Force Microscopy: What Is Achieved and What Is Needed. *Adv. Phys.* **1996**, *45*, 1–86.
38. Viani, M. B.; Pietrasanta, L. I.; Thompson, J. B.; Chand, A.; Gebeshuber, I. C.; Kindt, J. H.; Richter, M.; Hansma, H. G.; Hansma, P. K. Probing Protein-Protein Interactions in Real Time. *Nat. Struct. Biol.* **2000**, *7*, 644–647.
39. Yang, J.; Mou, J. X.; Shao, Z. F. Molecular Resolution Atomic Force Microscopy of Soluble Proteins in Solution. *Biochim. Biophys. Acta* **1994**, *1199*, 105–114.
40. Mou, J.; Yang, J.; Shao, Z. An Optical-Detection Low-Temperature Atomic-Force Microscope at Ambient Pressure for Biological Research. *Rev. Sci. Instrum.* **1993**, *64*, 1483–1489.
41. Czajkowsky, D. M.; Iwamoto, H.; Shao, Z. Atomic Force Microscopy in Structural Biology: From the Subcellular to the Submolecular. *J. Electron Microsc.* **2000**, *49*, 395–406.
42. Shao, Z.; Shi, D.; Somlyo, A. V. Cryo-Atomic Force Microscopy of Filamentous Actin. *Biophys. J.* **2000**, *78*, 950–958.
43. Zhang, Y.; Shao, Z.; Somlyo, A. P.; Somlyo, A. V. Cryo-Atomic Force Microscopy of Smooth Muscle Myosin. *Biophys. J.* **1997**, *72*, 1308–1318.
44. Hoh, J. H.; Lal, R.; John, S. A.; Revel, J. P.; Arnsdorf, M. F. Atomic Force Microscopy and Dissection of Gap Junctions. *Science* **1991**, *253*, 1405–1408.
45. Hoh, J. H.; Sosinsky, G. E.; Revel, J. P.; Hansma, P. K. Structure of the Extracellular Surface of the Gap Junction by Atomic Force Microscopy. *Biophys. J.* **1993**, *65*, 149–163.
46. Muller, D. J.; Schabert, F. A.; Buldt, G.; Engel, A. Imaging Purple Membranes in Aqueous Solutions at Sub-Nanometer Resolution by Atomic Force Microscopy. *Biophys. J.* **1995**, *68*, 1681–1686.
47. Muller, D. J.; Buldt, G.; Engel, A. Force-induced Conformational Change of Bacteriorhodopsin. *J. Mol. Biol.* **1995**, *249*, 239–243.
48. Wilchek, M.; Bayer, E. A. Avidin-Biotin Technology Ten Years On: Has It Lived Up to Its Expectations? *Trends Biochem. Sci.* **1989**, *14*, 408–412.
49. Schetters, H. Avidin and Streptavidin in Clinical Diagnostics. *Biomol. Eng.* **1999**, *16*, 73–78.
50. Reznik, G. O.; Vajda, S.; Cantor, C. R.; Sano, T. A Streptavidin Mutant Useful for Directed Immobilization on Solid Surfaces. *Bioconjugate Chem.* **2001**, *12*, 1000–1004.
51. Ylikotila, J.; Välimaa, L.; Takalo, H.; Pettersson, K. Improved Surface Stability and Biotin Binding Properties of Streptavidin Coating on Polystyrene. *Colloids Surf., B* **2009**, *70*, 271–277.
52. Gast, A. P.; Robertson, C. R.; Wang, S.-W.; Yatcilla, M. T. Two-Dimensional Streptavidin Crystals: Macropatterns and Micro-Organization. *Biomol. Eng.* **1999**, *16*, 21–27.
53. Schief, W. R.; Edwards, T.; Frey, W.; Koppenol, S.; Stayton, P. S.; Vogel, V. Two-Dimensional Crystallization of Streptavidin: In Pursuit of the Molecular Origins of Structure, Morphology, and Thermodynamics. *Biomol. Eng.* **1999**, *16*, 29–38.
54. Bailey, S. W. Cation Ordering and Pseudosymmetry in Layer Silicates. *Am. Mineral.* **1975**, *60*, 175–187.
55. Collins, D. R.; Catlow, C. R. A. Computer Simulation of Structures and Cohesive Properties of Micas. *Am. Mineral.* **1992**, *77*, 1172–1181.

56. Weber, P. C.; Ohlendorf, D. H.; Wendoloski, J. J.; Salemme, F. R. Structural Origins of High-Affinity Biotin Binding to Streptavidin. *Science* **1989**, *243*, 85–88.
57. Hendrickson, W. A.; Pahler, A.; Smith, J. L.; Satow, Y.; Merritt, E. A.; Phizackerley, R. P. Crystal Structure of Core Streptavidin Determined from Multiwavelength Anomalous Diffraction of Synchroron Radiation. *Proc. Natl. Acad. Sci. U. S. A.* **1989**, *86*, 2190–2194.
58. Reviakine, I.; Brisson, A. Streptavidin 2D Crystals on Supported Phospholipid Bilayers: Toward Constructing Anchored Phospholipid Bilayers. *Langmuir* **2001**, *17*, 8293–8299.
59. Scheuring, S.; Muller, D. J.; Ringler, P.; Heymann, J. B.; Engel, A. Imaging Streptavidin 2D Crystals on Biotinylated Lipid Monolayers at High Resolution with the Atomic Force Microscope. *J. Microsc.* **1999**, *193*, 28–35.
60. Bookin, A. S.; Drits, V. A. Factors Affecting Orientation of Oh-Vectors in Micas. *Clays Clay Miner.* **1982**, *30*, 415–421.
61. Mou, J. X.; Yang, J.; Shao, Z. F. Atomic-Force Microscopy of Cholera-Toxin B-Oligomers Bound to Bilayers of Biologically Relevant Lipids. *J. Mol. Biol.* **1995**, *248*, 507–512.
62. Zhang, R. G.; Westbrook, M. L.; Westbrook, E. M.; Scott, D. L.; Otwinowski, Z.; Maulik, P. R.; Reed, R. A.; Shipley, G. G. The 2.4 Angstrom Crystal Structure of Cholera-Toxin B Subunit Pentamer - Choleragenoid. *J. Mol. Biol.* **1995**, *251*, 550–562.
63. Stein, P. E.; Boodhoo, A.; Armstrong, G. D.; Cockle, S. A.; Klein, M. H.; Read, R. J. The Crystal Structure of Pertussis Toxin. *Structure* **1994**, *2*, 45–57.
64. Chayen, N. E.; Saridakis, E.; El-Bahar, R.; Nemirovsky, Y. Porous Silicon: An Effective Nucleation-Inducing Material for Protein Crystallization. *J. Mol. Biol.* **2001**, *312*, 591–595.
65. Sun, L. H.; Xu, C. Y.; Yu, F.; Tao, S. X.; Li, J.; Zhou, H.; Huang, S.; Tang, L.; Hu, J.; He, J. H. Epitaxial Growth of Trichosanthin Protein Crystals on Mica Surface. *Cryst. Growth Des.* **2011**, *10*, 2766–2769.
66. Helsel, A. J.; Brown, A. L.; Yamato, K.; Feng, W.; Yuan, L. H.; Clements, A. J.; Harding, S. V.; Szabo, G.; Shao, Z. F.; Gong, B. Highly Conducting Transmembrane Pores Formed by Aromatic Oligoamide Macrocycles. *J. Am. Chem. Soc.* **2008**, *130*, 15784–15785.
67. Lehn, J.-M. *Supramolecular Chemistry: Concepts and Perspectives*; VCH: New York, 1995.
68. Gilbert, B.; Huang, F.; Zhang, H. Z.; Waychunas, G. A.; Banfield, J. F. Nanoparticles: Strained and Stiff. *Science* **2004**, *305*, 651–654.
69. Czajkowsky, D. M.; Shao, Z. F. Supported Lipid Bilayers as Effective Substrates for Atomic Force Microscopy. *Methods Cell Biol.* **2002**, *68*, 231–241.
70. Henin, J.; Chipot, C. Overcoming Free Energy Barriers Using Unconstrained Molecular Dynamics Simulations. *J. Chem. Phys.* **2004**, *121*, 2904–2914.
71. Humphrey, W.; Dalke, A.; Schulten, K. VMD: Visual Molecular Dynamics. *J. Mol. Graphics* **1996**, *14*, 33–38.
72. Phillips, J. C.; Braun, R.; Wang, W.; Gumbart, J.; Tajkhorshid, E.; Villa, E.; Chipot, C.; Skeel, R. D.; Kale, L.; Schulten, K. Scalable Molecular Dynamics with NAMD. *J. Comput. Chem.* **2005**, *26*, 1781–1802.
73. MacKerell, A. D.; Bashford, D.; Bellott, M.; Dunbrack, R. L.; Evanseck, J. D.; Field, M. J.; Fischer, S.; Gao, J.; Guo, H.; Ha, S.; *et al*. All-Atom Empirical Potential for Molecular Modeling and Dynamics Studies of Proteins. *J. Phys. Chem. B* **1998**, *102*, 3586–3616.
74. Jorgensen, W. L.; Chandrasekhar, J.; Madura, J. D.; Impey, R. W.; Klein, M. L. Comparison of Simple Potential Functions for Simulating Liquid Water. *J. Chem. Phys.* **1983**, *79*, 926–935.